Vesiculation rates of obsidian domes inferred from H_2O concentration profiles

Jonathan M. Castro,[1] Michael Manga,[2] and Michael C. Martin,[3]

Received 9 July 2005; revised 16 September 2005; accepted 20 September 2005; published 5 November 2005.

[1] Explosivity of rhyolite domes depends on bubble nucleation and growth. To understand these processes, we measure millimeter-scale variations in H_2O by synchrotron Fourier transform infrared (FTIR) spectromicroscopy on interlayered obsidian-pumice samples. The H_2O contents of all samples are above the 1-atm solubility value ($\sim$0.10 wt.%) and decrease systematically towards vesicular zones, indicating that gas bubbles were growing and that degassing of melt to atmospheric pressure was incomplete. H_2O profiles are compared with models for water diffusion in order to constrain the temporal scale of vesiculation. Diffusion timescales range from 0.4 to 15 days, and represent the time between bubble nucleation and quenching. We use these results to estimate the duration of volatile exsolution and evaluate the timing of the formation of explosion pits frequently found on the surfaces of obsidian domes, though never witnessed. **Citation:** Castro, J. M., M. Manga, and M. C. Martin (2005), Vesiculation rates of obsidian domes inferred from H_2O concentration profiles, *Geophys. Res. Lett.*, *32*, L21307, doi:10.1029/2005GL024029.

1. Introduction

[2] Volatile exsolution and separation from magma (degassing) is arguably the most important process governing the dynamics of volcanic eruptions. Vesiculation is the critical first step in the degassing process, and one that drives nearly all volcanic eruptions. Bubbles nucleate when the melt becomes supersaturated in volatile components (e.g., H_2O). They continue to grow by diffusive transfer of gas species into bubbles and by the expansion of these gases as the magma decompresses.

[3] Vesiculation in effusive (lava-dome forming) eruptions can take days to months due to low decompression rates and small supersaturation. Nonetheless, effusive magmas may remain supersaturated [e.g., *DeGroat-Nelson et al.*, 2001] upon extrusion and retain the potential to generate dangerous volcanic blasts [*Fink and Kieffer*, 1993].

[4] Lava dome explosivity is a consequence of the buildup of stresses as H_2O exsolves into growing bubbles [*Eichelberger*, 1995]. Evaluating the explosive potential of lava domes therefore requires constraints on the timescales of H_2O diffusion out of the melt and into bubbles. Here we measure H_2O concentration profiles on obsidians that have been quenched while vesiculating. We use these profiles to quantify the timescales of diffusion and vesiculation. This temporal information, in turn, is used to infer the timing of endogenic explosions on obsidian domes.

2. Sample Descriptions, Methods and Measurements

[5] We analyzed three samples from two late Holocene flows in California (Figure 1). These interlayered obsidian-pumice assemblages were collected near the margins of coarse pumice outcrops, which have been interpreted to be the remains of pumiceous diapirs that rose buoyantly within the flow interior to the surface during flow emplacement [*Fink et al.*, 1992]. Each sample contains μm-scale flow bands made visible by variations in the content (<5 vol.%) of pyroxene microlites. Bands are parallel to the boundaries between glassy and vesicular rhyolite. Two samples (NC-1, 2) come from North Coulee, Mono Craters and each consists of a planar piece of obsidian bound on both sides by pumice. A third sample (BGF2), from Big Glass Mountain, is an 8 mm-thick obsidian layer (BGM; Figure 1c).

[6] H_2O concentrations were measured by synchotron Fourier transform infrared (FTIR) spectromicroscopy at the Advanced Light Source Facility at Lawrence Berkeley National Lab. The FTIR instrument utilizes an IR beam with a diffraction-limited diameter of 3–10 μm [*Martin and McKinney*, 1998]. The uncertainty in spot position is $\pm$2 μm. Line maps of H_2O content were made across the glassy zones between bounding vesicular zones with the aid of a motorized stage. Traverses were oriented roughly normal to the interface between pumice and glass. Measurements were made at intervals of 20 μm (samples NC-1, NC-2) and 40 μm (BGF2) on doubly-polished wafers cut perpendicular to banding and hence, interfaces between vesicular and dense glassy zones. Wafer thickness was measured along each profile with a digital micrometer at a precision of $\pm$2 μm. Thickness varied from 105 to 112 μm on sample NC-1, 90 to 100 μm on NC-2, and 330 to 384 μm on BGF2. Total H_2O concentrations were determined from the intensity of the 3750 cm^{-1} absorption band [*Newman et al.*, 1986]. Analytical error is estimated to be $\pm$0.005 wt.% based on the repeat analysis of multiple spots. H_2O concentrations were corrected for the volume fraction of pyroxene microlites, however, variability due to changing microlite contents is less than the analytical uncertainty.

[7] Figure 2 shows H_2O profiles and accompanying photomicrographs scaled to match the different transects. Data gaps represent analyses that were omitted due to their malformed spectral peaks. The NC-1 profile is characterized

[1]Department of Mineral Sciences, Smithsonian Institution, Washington, D. C., USA.
[2]Department of Earth and Planetary Science, University of California, Berkeley, California, USA.
[3]Advanced Light Source, Lawrence Berkeley National Laboratory, Berkeley, California, USA.

0094-8276/05/2005GL024029

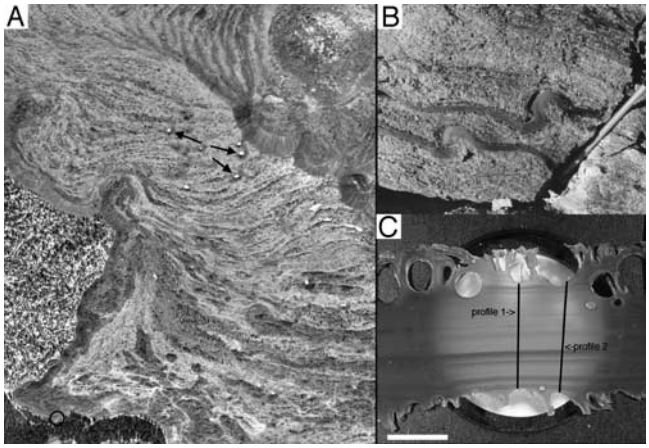

Figure 1. (a) Aerial photograph of Big Glass Mountain, CA. Dark lava is coarsely vesicular rhyolite. The sample locality of BGF2 is shown in the circle. Note explosion pits (arrows). Horizontal scale is approximately 750 m. North direction is up. (b) Folded obsidian layers within pumice. Note pencil at right for scale. (c) Obsidian wafer prepared from sample BGF2 extracted from the outcrop shown in B. Scale bar is 3 mm long. FTIR profiles are shown as black lines.

by a narrow range of H_2O across the center of the band ($\sim$0.16–0.17 wt.%), and a decrease in H_2O content towards the vesicular zones. Sample NC-2 (Figure 2b) is characterized by two peaks positioned on either side of a central segment with variable H_2O contents. The central region corresponds to a zone of collapsed vesicles, which appears dark in the photomicrograph. The left side of this profile shows an increase in H_2O towards the vesicular margin. The two BGF2 profiles have similar forms defined by two peaks that bound a broad intervening trough (Figures 2c and 2d). H_2O content drops sharply outside the peaks towards the interfaces between obsidian and pumice. That the profiles on BGF2 are similar suggests that the H_2O concentration gradients are laterally continuous and perpendicular to both of the vesiculation boundaries.

3. Implications for Vesiculation

[8] H_2O concentrations measured here are similar to those determined on effusive obsidians in earlier studies [e.g., *DeGroat-Nelson et al.*, 2001] and are consistent with equilibration pressures between 0.5 and 0.1 MPa [e.g., *Silver et al.*, 1989]. Such pressures correspond to depths between 30 m and the surface of the lava flow, respectively. Given an approximate flow thickness of 100 m (on BGM flow), the measured volatile concentrations reflect the latest stages of degassing and final decompression during emplacement.

[9] Interestingly, H_2O concentrations are not uniform across the bands. Most profiles show a drop in H_2O at the boundaries between obsidian and pumice. A mass-volume balance shows that the amount of H_2O lost ($\sim$0.05–0.08 wt.%), measured directly on the profiles by integrating across the depleted zones next to the pumice margins, can be accounted for by the volume of the $\sim$1 mm diameter vesicles next to the obsidian-pumice interface. Bubble volume was determined from the bubble diameter assuming a spherical shape. Slight distortions of bubble shapes from spherical result in an estimated volume error of about 10%. The mass-balance calculation assumes ideal gas behavior of H_2O at 0.1 MPa and holds for temperatures ranging from the glass transition (T_g; $\sim$750°C) [*Castro et al.*, 2005] to a feasible eruption temperature of 850°C [e.g., *Gibson and Naney*, 1992]. The balance between the mass lost from marginal zones and the observed volume of bubbles suggests that bubble growth was dominated by volatile diffusion into bubbles and that growth due to decompression of

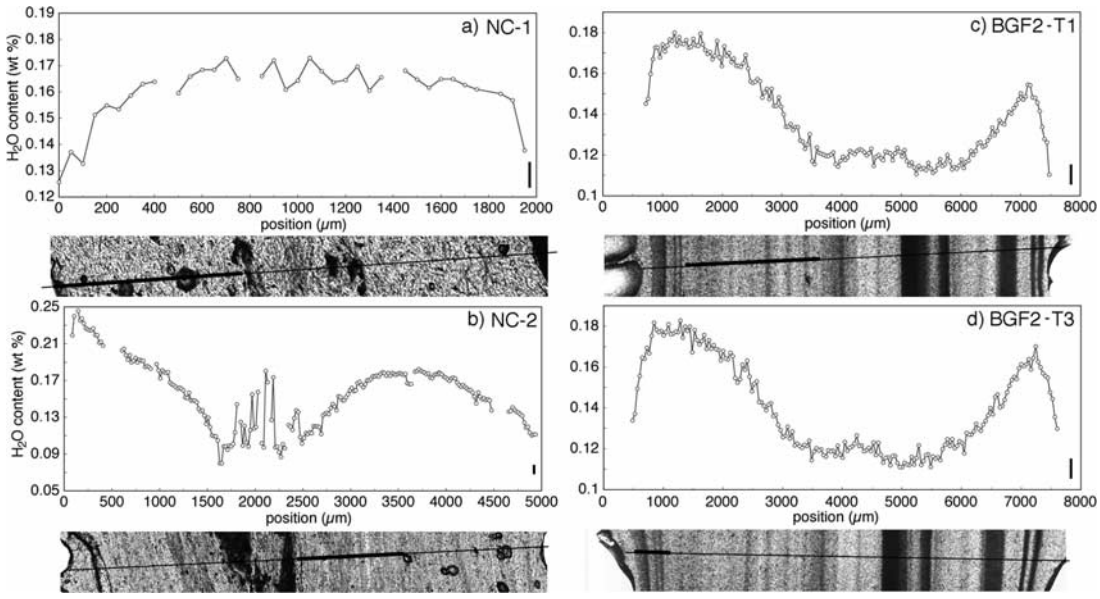

Figure 2. H_2O-concentration profiles. Vertical bars in each graph show the analytical error. Photomicrographs are scaled to the position axis on each overlying profile. Black lines shows the measurement traverse. Bold lines superimposed on profile lines show the segments modeled by the diffusion equation.

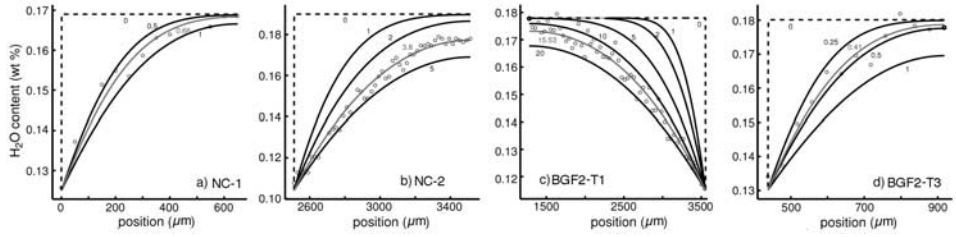

Figure 3. Measured H_2O concentration (circles) and model diffusion profiles for different diffusion timescales (curves). Dashed curves show initial conditions. Diffusion times in days are shown as labels on model curve. Best-fit solution is the gray curve.

preexisting bubbles was relatively unimportant. Given these relations, we interpret the profiles to be the result of diffusion of H_2O from the melt into newly created bubbles.

[10] In contrast to profiles on BGF2 and NC-1, the H_2O content at the left margin of NC-2 appears to increase toward the vesicular margin and shows only a slight decrease in the last two points. This trend may be a sign of secondary hydration.

[11] In most cases, exsolution of H_2O into bubbles is indicated by H_2O concentrations increasing away from vesicular regions. The interior of sample BGF2 is, however, devoid of vesicles despite being depleted in H_2O. We suggest that the degassed, bubble-free interior of this sample was once vesicular or fragmental [e.g., *Gonnermann and Manga*, 2003] but has since undergone either bubble collapse and annealing [e.g., *Westrich and Eichelberger*, 1994] or rewelding of fragmented magma [e.g., *Tuffen et al.*, 2003]. This interpretation is supported by the bubble-collapse textures and H_2O-depleted interior of sample NC-2 (Figure 2b). The elevated H_2O spikes remaining within the collapsed vesicular zone of NC-2 may have resulted from volatile resorption during bubble collapse [*Westrich and Eichelberger*, 1994].

4. Vesiculation Timescales

[12] Diffusion profiles are preserved in obsidian due to cooling of the melt across the glass transition temperature (T_g) prior to the complete diffusion of H_2O. *Zhang et al.* [1991] note that even though OH^- is the dominant species in extensively degassed rhyolite melts, it is not the dominant diffusing species as interconversion of OH^- to molecular H_2O occurs prior to and possibly during exsolution. Preservation of diffusion profiles will also be promoted by the shift in T_g due to dewatering at the bubble-melt interface. For example, a decrease in H_2O from 0.2 to 0.1 wt.% will result in about a 50°C increase in T_g [*Hess and Dingwell*, 1996].

[13] The data in Figure 2 can be modeled to determine the diffusion timescale. Diffusion timescales are, in turn, a measure of the vesiculation timescale considering that diffusion begins with the nucleation of bubbles, continues during bubble growth, and ceases at the time of quenching.

[14] The shapes of diffusion profiles are a function of the concentration gradient and diffusion rate of H_2O, which in turn, depends on the species-dependant diffusivity (D). Diffusivity has an Arrhenian dependence on temperature (T), is a weak function of pressure (P), and depends on the H_2O content (C) [e.g., *Zhang et al.*, 1991; *Zhang and Behrens*, 2000]. We solve numerically the 1D diffusion equation:

$$\frac{\partial C}{\partial t} = \frac{\partial}{\partial x}\left(D(C,T,P)\frac{\partial C}{\partial x}\right) \quad (1)$$

where $D(C, T, P)$ is the diffusivity of H_2O in rhyolite melt [*Zhang and Behrens*, 2000]. Although bubbles are spherical, the pervasive bubble layering and continuity of water content parallel to the bands is best modeled with a Cartesian coordinate system. Model calculations assume constant T = 850°C and P = 0.1 MPa. The initial H_2O content is fixed to be the maximum measured value. Boundary conditions include zero mass flux away from the bubble melt interface, and a value at the bubble surface that is equal to the minimum value measured on the profile. The best-fit model is the one that minimizes the mean absolute error.

[15] Figure 3 compares measurements and model predictions for different diffusion timescales. We modeled only profile segments that show a clear "flattening" of the H_2O content away from the vesicular interface. This provides a relatively unambiguous choice for the initial H_2O content in models. The four profiles shown are representative of the range of diffusion patterns, from relatively large drops in H_2O over a narrow distance to more gradual H_2O decreases spread over greater distance. Best-fit diffusion timescales range from about 0.4 to 15 days. If modeled diffusion times represent vesiculation timescales, then this range could reflect differences between the time of bubble nucleation and quenching (i.e., passage across T_g). Short timescales of NC-1 and BGF2-T3, which correspond to marginal vesiculation zones, imply that these vesiculation events were the most recent and diffusion occurred for a short time prior to cooling across T_g. The longer timescales determined for BGF2-T1 and NC-2 profiles suggest longer and possibly earlier vesiculation events than the ones preserved on the edges.

[16] A source of uncertainty in our calculations is the choice of a melt temperature, which directly affects D. Thus, timescales obtained from modeling should be viewed as first-order. At the very least they provide the relative timescales. Timescales of days determined here overlap with those of the 1980–86 Mount St. Helens (MSH) dome extrusions in which dacite lava vesiculated 1 to 3 days after extrusion [*Swanson et al.*, 1987]. This similarity in timescales provides some validation of our calculations

given that the bulk compositions of the groundmass melt of the MSH dome are similar to that of many rhyolitic obsidians.

5. Hazard Implications

[17] From a hazards perspective, it is important to understand the mechanisms and timescale of vesiculation within obsidian flows as this affects the timing of explosions occurring at or near their surfaces [e.g., *Jensen*, 1993]. Endogenic explosions on the surfaces of domes occur due to the buildup of gas pressure within the flow, eventually leading to internal pressures in excess of the strength of the overlying crust [e.g., *Fink et al.*, 1992]. The generally circular (unstrained) form of explosion craters suggests that explosions occur sometime after the flow ceases (Figure 1) [*Fink et al.*, 1992]. Other field observations [e.g., *Jensen*, 1993] indicate that explosions originate from a volatile-charged layer of coarse pumice underlying a dense obsidian layer at depths between 15 and 20 m. H_2O concentrations measured on a core drilled through this layer ($\sim$0.3–0.5 wt.%) [*Westrich et al.*, 1988] are elevated compared to the contents of surface lavas. Such internal H_2O concentrations can provide enough vapor pressure to exceed the surface crust strength and generate an explosion [*DeGroat-Nelson et al.*, 2001].

[18] We can estimate the timing of explosions from the vesiculation timescales inferred from diffusion models. We assume that prior to explosive venting, volatiles exsolve from the melt into newly nucleated or preexisting bubbles. The expansion of bubbles increases the pressure of the gas and magma contained below a crust. We assume that an explosion will occur when the strength of the crust is overcome by some critical internal gas pressure [*Fink and Kieffer*, 1993]. Crust strengths on obsidian flows vary from about 0.1 to 0.5 MPa, depending on their thickness [*Fink and Griffiths*, 1998]. Considering a crust strength of 0.3 MPa, consistent with a flow depth of about 15 m (the average depth of explosion craters), a mass of about 0.2 wt.% H_2O must exsolve to produce the vapor pressure necessary to rupture the crust.

[19] Average H_2O-loss, or exsolution rates can be determined from the total decline in H_2O measured directly on concentration profiles divided by their respective diffusion times. We determine rates of volatile loss between 2×10^{-4} to 3×10^{-3} wt.% hr^{-1}. These are integrated exsolution rates because at any particular time the rates of diffusion and volatile loss are controlled by the continually changing concentration gradient (equation (1)). Given these exsolution rates, the time required to exsolve 0.2 wt.% of H_2O and consequently drive an explosion, will range from about 3 to 40 days.

[20] The precise timing of an explosion relative to the onset of effusion is difficult to determine because we do not know when gas pressure begins to build up in the interior of the flow. The proximal and distal positions of coarse pumice diapirs (Figure 1), which are also a manifestation of the build up of gas in flow interiors [e.g., *Fink et al.*, 1992], suggest that internal degassing occurs early and continually throughout emplacement. However, unlike the diapiric rise of pumice bodies, explosions appear to happen in the waning stages if not after flow advance. Thus, timescales of days to weeks calculated above may represent the time interval leading up to or just following flow cessation.

[21] That explosions apparently do not occur during flow advance is intriguing, and may suggest a fundamental difference between the mechanisms that form diapiric structures and endogenic explosions. One possibility is that continuous disruption of the crust by viscous forces generated during flow may aid in the migration of volatile-charged, low-density pumice diapirs to the surface leading to passive extrusion and degassing of these bodies. In addition, once the flow has stopped, the pathways for gas escape formed by shearing and disruption of the crust may be greatly reduced, thereby causing a greater buildup of gas pressure within the flow and ultimately explosive decompression.

6. Concluding Remarks

[22] Detailed measurements of H_2O in flow-banded obsidians indicate that the H_2O contents in effusive obsidians are heterogeneous and the patterns of concentration are consistent with diffusion of H_2O out of the melt and into bubbles rather than from hydration from external sources. The concentration profiles, combined with textural features such as collapsed and primary vesicles, suggest that bubble collapse and complete erasure of former degassing channels is a feasible degassing mechanism in advancing obsidian flows. Exsolution rates inferred from modeled diffusion profiles indicate vesiculation timescales on the order of hours to days and imply that endogenic explosions may occur days to weeks after flow emplacement.

[23] **Acknowledgments.** We thank B. Cameron, H. Gonnermann, A. Rocholl, K. Roggensack, and A. Rust for comments. JC was supported by the Alexander von Humboldt Foundation; MM was supported by NSF EAR027471.

References

Castro, J. M., D. B. Dingwell, A. R. L. Nichols, and J. E. Gardner (2005), New insights on the origin of flow bands in obsidian, in *Lava Flow Dynamics*, edited by M. Manga and G. Ventura, *Geol. Soc. Am. Spec. Pap.*, *396*, 55–65.

DeGroat-Nelson, P. J., B. I. Cameron, J. H. Fink, and J. R. Holloway (2001), Hydrogen isotope analysis of rehydrated silicic lavas: Implications for eruption mechanisms, *Earth Planet Sci. Lett.*, *185*, 331–341.

Eichelberger, J. C. (1995), Silicic volcanism: Ascent of viscous magmas from crustal reservoirs, *Annu. Rev. Earth Planet. Sci.*, *23*, 41–63.

Fink, J. H., and R. W. Griffiths (1998), Morphology, eruption rates, and rheology of lava domes: Insights from laboratory models, *J. Geophys. Res.*, *103*, 527–545.

Fink, J. H., and S. W. Kieffer (1993), Estimate of pyroclastic flow velocities resulting from explosive decompression of lava domes, *Nature*, *363*, 612–615.

Fink, J. H., S. W. Anderson, and C. R. Manley (1992), Textural constraints on effusive silicic volcanism: Beyond the permeable foam model, *J. Geophys. Res.*, *97*, 9073–9083.

Gibson, R. G., and M. T. Naney (1992), Textural development of mixed, finely porphyrititc silicic volcanic rocks, Inyo Domes, eastern California, *J. Geophys. Res.*, *97*, 4541–4559.

Gonnermann, H., and M. Manga (2003), Explosive volcanism may not be an inevitable consequence of magma fragmentation, *Nature*, *426*, 432–435.

Hess, K.-U., and D. B. Dingwell (1996), Viscosities of hydrous leucogranitic melts: A non-Arrhenian model, *Am. Mineral.*, *81*, 1297–1300.

Jensen, R. A. (1993), Explosion craters and giant gas bubbles on Holocene rhyolite flows at Newberry Crater, Oregon, *Oregon Geol.*, *55*, 13–19.

Martin, M. C., and W. R. McKinney (1998), The first synchotron infrared beamlines at the advanced light source: Microspectroscopy and fast timing, *Proc. Mater. Res. Soc.*, *524*, 11.

Newman, S., E. M. Stolper, and S. Epstein (1986), Measurement of water in rhyolitic glasses: Calibration of an infrared spectroscopic technique, *Am. Mineral.*, *71*, 1527–1541.

Silver, L. A., P. D. Ihinger, and E. Stolper (1989), The influence of bulk composition on the speciation of water in silicate glasses, *Contrib. Mineral. Petrol.*, *104*, 142–162.

Swanson, D. A., D. Dzurisin, R. T. Holcomb, E. Y. Iwatsubo, W. W. Chadwick Jr., T. J. Casadevall, J. W. Ewert, and C. C. Heliker (1987), Growth of the lava dome at Mount St. Helens, Washington, in *Emplacement of Silicic Domes and Lava Flows*, edited by J. H. Fink, *Spec. Pap. Geol. Soc. Am.*, *212*, 1–16.

Tuffen, H., D. B. Dingwell, and H. Pinkerton (2003), Repetitive fracture and healing in silicic magmas generates flow banding and earthquakes?, *Geology*, *31*, 1089–1092.

Westrich, H. R., and J. C. Eichelberger (1994), Gas transport and bubble collapse in rhyolitic magma: An experimental approach, *Bull. Volcanol.*, *56*, 447–458.

Westrich, H. R., H. W. Stockman, and J. C. Eichelberger (1988), Degassing of rhyolitic magma during the ascent and emplacement, *J. Geophys. Res.*, *93*, 6503–6511.

Zhang, Y., and H. Behrens (2000), H_2O diffusion in rhyolitic melts and glasses, *Chem. Geol.*, *169*, 243–262.

Zhang, Y., E. M. Stolper, and G. J. Wasserburg (1991), Diffusion of water in rhyolititc glasses, *Geochim. Cosmochim. Acta.*, *55*, 441–456.

J. M. Castro, Department of Mineral Sciences, Smithsonian Institution, P.O. Box 37012, Washington, DC 20012–7012, USA. (castroj@si.edu)

M. Manga, Department of Earth and Planetary Science, University of California, Berkeley, Berkeley, CA 94720–4767, USA.

M. C. Martin, Advanced Light Source, Lawrence Berkeley National Laboratory, Berkeley, CA 94720–8226, USA.